Electronic Supplementary Information

A Green synthesis of highly luminescent carbon dots from itaconic acid and its application as an efficient sensor for Fe^{3+} ions in aqueous medium

Vadivel Ramanan,[a] Supriya Hegde Subray,[b] and Perumal Ramamurthy*[a]

[a]*National Centre for Ultrafast Processes, University of Madras, Taramani Campus, Chennai - 600113, Tamilnadu, India*

[b]*Department of Chemistry, Mangalore University, Mangalagangothri, Konaje, Mangalore, Karnataka – 574199, India.*

*Corresponding Author

prm60@hotmail.com

The electronic supplementary information contains

27 pages

8 Figures

9 Tables

CONTENTS

Experimental Methods

Chemicals and reagents

Itaconic acid (IA) is obtained from Sigma Aldrich. Ethylenediamine (EDA) was purchased from Qualigens. Quinine sulfate (98%, suitable for fluorescence) was supplied by Fluka. KCl was used to adjust the ionic strength for ionic strength susceptibility experiments and that was purchased from Qualigens. For pH dependent fluorescence studies, pH of the N-CDs solution was adjusted using sodium hydroxide and sulfuric acid, both were purchased from Qualigens. The metal ion salts were purchased from Sigma-Aldrich. Cellulose ester dialysis membrane (Spectra/Por, Float-A-Lyzer G2, 1KD MWCO) was purchased from Spectrum Labs. Deionized Water (DIW) was obtained from a Aquelix 5 water purification system, and used throughout the work. Water samples from various sources were collected to check the sensing ability of the CDs at different systems. Mineral water (MW) is obtained from Bisleri, India. Pond water (PW) is collected from the lotus pond of Adhipurishwarar temple, Pallikaranai, Chennai, India (12°56'5" N, 80°12'15" E). Lake water (LW) and sea water (SW) were collected from the Velachery lake, Chennai, India (12°59'15" N, 80°30'45" E), and from the Marina beach, Chennai, India (13°03'15" N, 80°17'01" E) respectively. Tap water (TW) sample is obtained from our lab. The water samples were filtered through a membrane (pore size: 0.45 μm) filter paper and centrifuged at 15,000 rpm for 30 min before analysis. The pH of water samples were adjusted to pH 7 by adding either dil. HCl or NaOH. KSCN used for colorimetric analysis of trace Fe^{3+} was purchased from Qualigens.

Instruments used for characterization

The size, morphology, and the selected area electron diffraction (SAED) pattern of the as prepared CDs were measured using a FEI Tecnai-G2 TEM instrument. Prior to TEM measurements, the synthesized CDs were carefully deposited onto a 400-mesh C-coated Cu grid and the excess solvents were evaporated at ambient temperature and pressure. Raman spectrum was recorded using a Laser Raman microscope-RAMAN 11i (Nanophoton Corp., Japan) by excitation at 532 nm. XPS measurements were obtained using Thermoscientific, MULTILAB 2000 spectrometer with monochromatized Al Kα X-rays (energy: 1486.6 eV). Spectra in the required binding energy range were collected, and an average spectrum was taken. The binding energy was calibrated with respect to the adventitious C 1s feature. The surface functional

groups on CDs were identified using Bruker, Vertex 70 Fourier transform infrared spectrometer at ATR mode.

Instruments used for photophysical investigation

UV-Vis absorption spectrum was recorded with Cary 100 Bio UV-Visible double beam spectrophotometer. PL, excitation and 3D contour spectra were recorded by a HORIBA JOBIN YVON Fluoromax 4P spectrofluorometer. The relative fluorescence quantum yield (QY) was calculated by comparing the integrated PL intensities (excited at 355 nm) and the absorbance values of CDs at 355 nm with those of the reference quinine sulfate. The fluorescence decay measurements were carried out using time correlated single photon counting (TCSPC) technique with microchannel plate photomultiplier tube (MCP-PMT) as a detector and a 375 nm (IRF: 229 ps) light emitting diode (LED) and second harmonic output (385 nm) of Ti-Sapphire femtosecond laser (IRF: 50 ps) as excitation sources. The TCSPC data analysis was carried out by the software provided by IBH (DAS-6), which is based on reconvolution technique using iterative non-linear least square methods. Quality of the fit is normally identified by the reduced χ^2, weighed residuals, and the autocorrelation function of the residuals. The intensity-weighted mean lifetime (τ_{mean}), the mean time delay of photon emission after the picosecond laser pulse was calculated according to

$$\tau_{mean} = \left[\frac{\sum \alpha_i \tau_i^2}{\sum \alpha_i \tau_i}\right]$$

Where, the α_i represents the fractional weights of the various decay time components, τ_i of the multi-exponential fitting.

Microwave synthesis of luminescent N-CDs

About 1g of IA was added to 20 mL of 15 % aqueous EDA in a 250 mL beaker. The beaker is then kept in a domestic microwave oven at 600 W for 2 min and 50 s. Then the beaker is allowed to cool naturally. Appearance of concentrated yellow solution infers the formation of CDs. The solution is dried and re-dissolved in 20 mL of ethanol. Dil. H_2SO_4 is then added drop-wise to precipitate the unreacted EDA as ethylene diammonium sulfate. It is then filtered through a Whatman 40 grade filter paper. The resultant clear yellow filtrate is then transferred into a polycarbonate centrifuge tube and subjected to centrifugation (REMI) at 15,000 rpm for 20

minutes in order to remove larger particles. The resulting clear centrifugate is then transferred into a pre-treated, cellulose ester dialysis membrane of 10 mL capacity. Dialysis was carried out for 48 h to remove any small molecules and products due to partial carbonization. The outer buffer was changed for every 4 hrs. Then the dialysate is collected and dried under vacuum using Equitron-Roteva, India to obtain solid CDs. Desired amount of obtained CDs were re-dissolved in water and used for further studies.

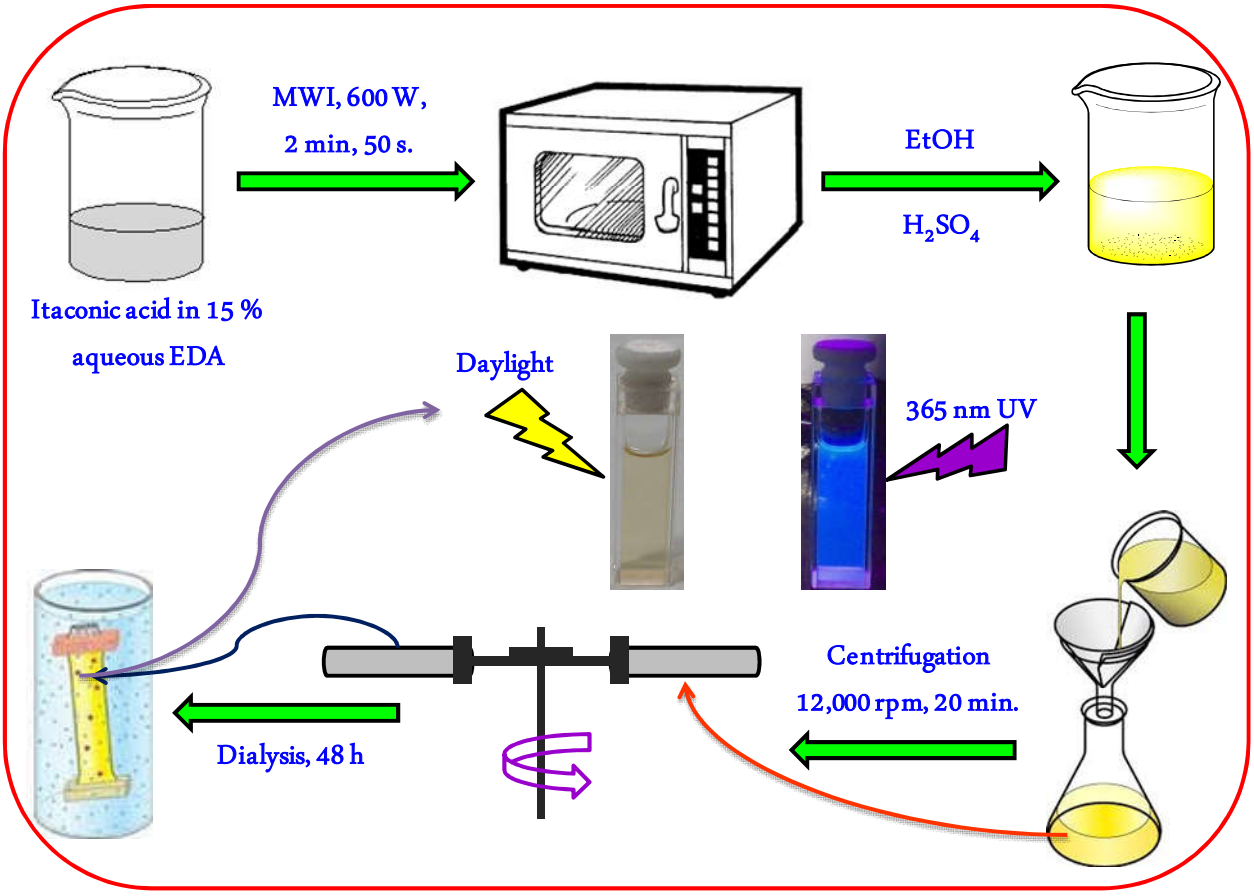

Scheme S1. Schematic representation for the synthesis of N-CDs from IA.

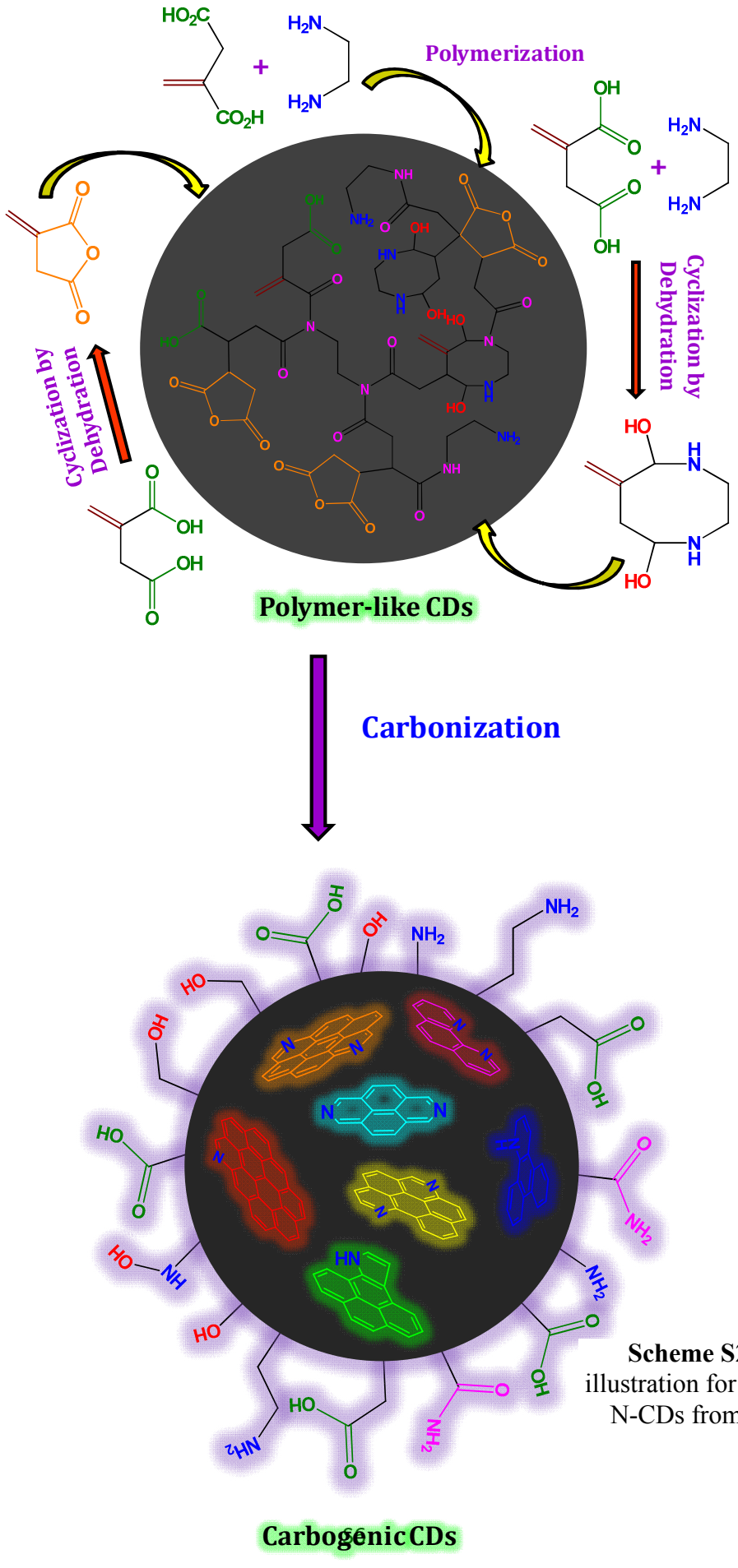

Scheme S2. Schematic illustration for the formation of N-CDs from IA and EDA.

Table S1. Optimization of synthetic conditions for the production of N-CDs from IA.

S. No.	MW Power (W)	Time of Irradiation	% of EDA	QY (%)
1	600	3 min 5 sec	5	24.7
2	600	3 min 15 sec	10	27.9
3	**600**	**2 min 50 sec**	**15**	**29.9**
4	600	3 min 20 sec	20	24.2

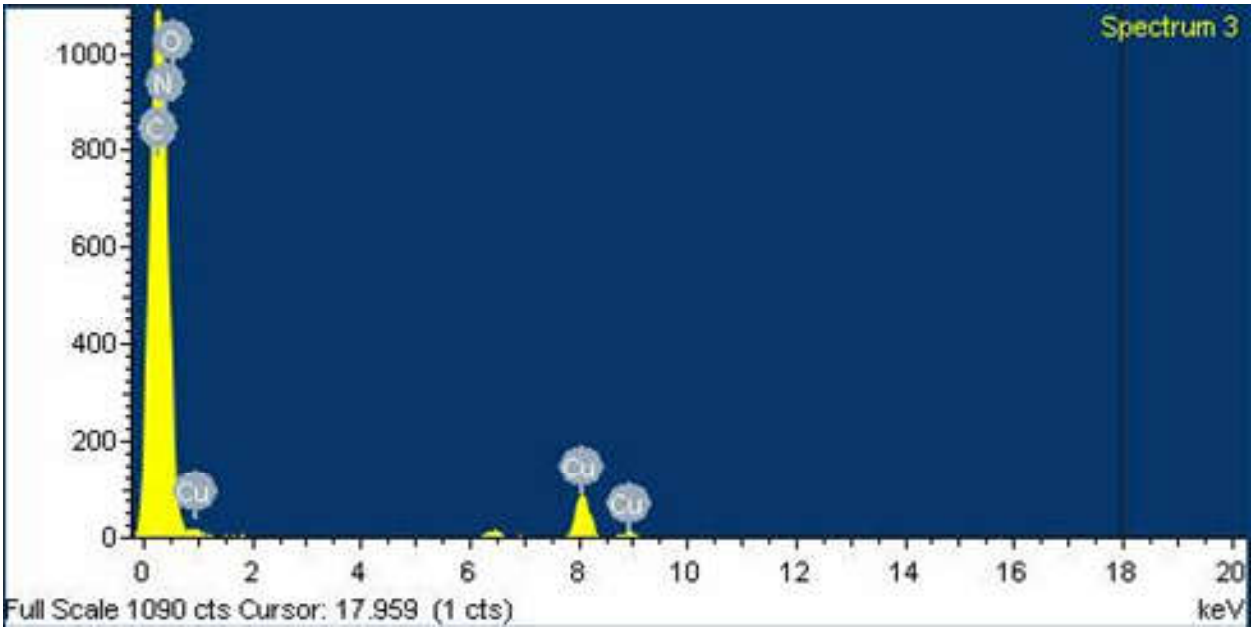

Figure S1. EDAX Spectrum of N-CDs showing the presence of C, N, and O.

Table S2. Comparison of nitrogen contents of previously reported N-CDs with that of IA-derived N-CDs.

S. No.	Nitrogen Precursor	Synthesis Method	% N	Ref.
1	PEG-diamine	Hydrothermal	Trace	1
2	EDA	Hydrothermal	Trace	2
3	EDA	Hydrothermal	Trace	3
4	Tris	Hydrothermal	Trace	4
5	Monkey Grass	Hydrothermal	NA	5
6	Histidine	Microwave-assisted Hydrothermal	NA	6
7	Ammonia	Hydrothermal	NA	7
8	Lemon Juice	Hydrothermal	NA	8
9	Guanidinium chloride	Heating	NA	9
10	Ortho-phosphorylethanolamine	Hydrothermal	NA	10
11	Egg Shell Membrane	Microwave	1.60	11
12	tribute chrysanthemum	Hydrothermal	1.98	12
13	EDA	Hydrothermal	3.24	13
14	Methionine	Hydrothermal	4.02	14
15	Coriander Leaves	Hydrothermal	4.07	15
16	Garlic	Hydrothermal	4.32	16
17	L-Cysteine	Hydrothermal	4.85	17
18	ZIF-8C (MOF-derived material)	Acid Vapour Cutting	4.90	18

19	Ammonium Citrate	Hydrothermal	5.35	19
20	Heparin Sodium	Hydrothermal	5.49	20
21	Ammonium Hydroxide	Hydrothermal	6.37	21
22	Ammonia	Hydrothermal	6.80	22
23	Di-ammonium hydrogen phosphate	Hydrothermal	7.73	23
24	Nescafe instant coffee	Extraction	7.8	24
25	Urea	Microwave	8.49	25
26	L-Glutamate	Hydrothermal	10.15	26
27	L-Glutamic acid	Microwave	10.42	27
28	ATP	Hydrothermal	11.59	28
29	Chitosan + EDA	Mircrowave	11.75	29
30	Poly-ethyleneimine	Hydrothermal	13.23	30
31	EDTA + Urea	Solvothermal	13.73	31
32	N-(b-aminoethyl)-c-aminopropylmethyl-dimethoxysilane	Solvothermal	13.93	32
33	BSA	Hydrothermal	14.0	33
34	**EDA**	**Microwave**	**14.0**	**This Work**
35	EDA	Solvothermal	17.5	34
36	Chitosan + EDA	Mircrowave	18.83	29

*NA = Not Available (but the % N is less than that of IA-derived N-CDs by the visual inspection of XPS survey spectrum).

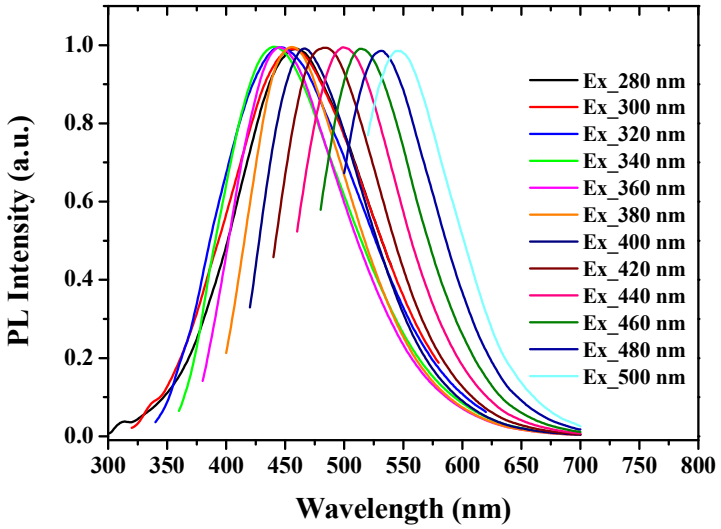

Figure S2. Normalized PL spectra of N-CDs excited at various wavelengths.

Quantum yield calculations

Quinine sulfate, QS (0.1N H_2SO_4 as solvent; Known QY=0.54) was chosen as standard. The QYs of CDs (in water) were calculated by two different methods.

1. The QY was determined by reference point method.

$$QY_{sam} = QY_{ref} (I_{sam}/I_{ref}) (A_{ref}/A_{sam}) (n_{sam}/n_{ref})^2 \rightarrow (1)$$

Where I is the measured integrated emission intensity, n is the refractive index of the solvent, and A is the absorbance. The subscript "ref" refers to standard with known QY and "sam" for the sample. In order to minimize re-absorption effects, absorption in the 1cm fluorescence cuvette was kept below 0.10 at the excitation wavelength (355 nm).

2. The QY was determined by slope method using quinine sulfate as the reference:

From the integrated photoluminescence intensity and the absorbance value [several values (less than 0.1 at excitation wavelength) built the curve] of the samples with that of the references.

The equation is:

$$QY_{sam} = QY_{ref} (K_{sam}/K_{ref})(n_{sam}/n_{ref})^2 \rightarrow (2)$$

Where, K is the slope determined by the curves and n is the refractive index. The subscript "ref" refers to the standards and "sam" refers to the unknown samples. For these aqueous solutions, $n_{sam}/n_{ref} = 1$.

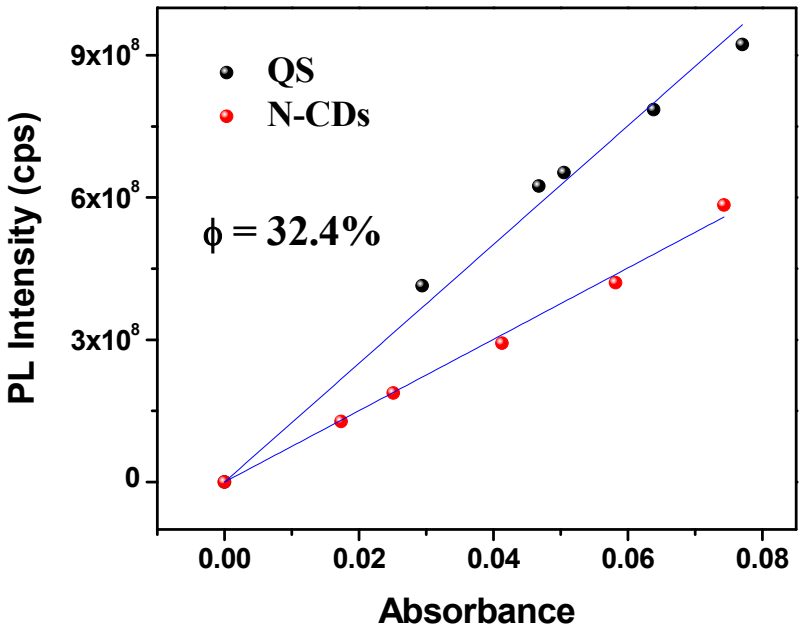

Figure S3. Slope method for the calculation of fluorescence quantum yield.

Table S3. Slope method for the calculation of fluorescence quantum yield.

$Slope_{sam}$	$Slope_{ref}$	$(n_{sam}/n_{ref})^2$	ϕ_{sam}	ϕ_{ref}
7.53×10^9	1.25×10^{10}	1	0.546	0.324
			Graphical Quantum Yield	**32.4%**

Table S4. Quantum yield calculated by reference point measurements (Using equation 1).

Quinine Sulfate		N-CDs		I_{sam}/I_{ref}	A_{ref}/A_{sam}	$(n_{sam}/n_{ref})^2$	ϕ_{ref}	ϕ_{sam}
Absorbance	**Integrated Area of Emission Spectrum**	**Absorbance**	**Integrated Area of Emission Spectrum**					
0.031	4.06×10^8	0.017	1.28×10^8	0.314	1.759	1	0.54	0.298
0.031	4.06×10^8	0.025	1.87×10^8	0.461	1.215	1	0.54	0.302
0.031	4.06×10^8	0.041	2.92×10^8	0.719	0.740	1	0.54	0.287
0.031	4.06×10^8	0.058	4.20×10^8	1.034	0.525	1	0.54	0.293
0.031	4.06×10^8	0.074	5.84×10^8	1.438	0.411	1	0.54	0.319
							Average	0.299
							Calculated Quantum Yield (%) after rounded off	**30.0**

The quantum yield obtained from graphical method and that is obtained from the mean of several reference point measurements are closely matches which shows the quality of the experiments.

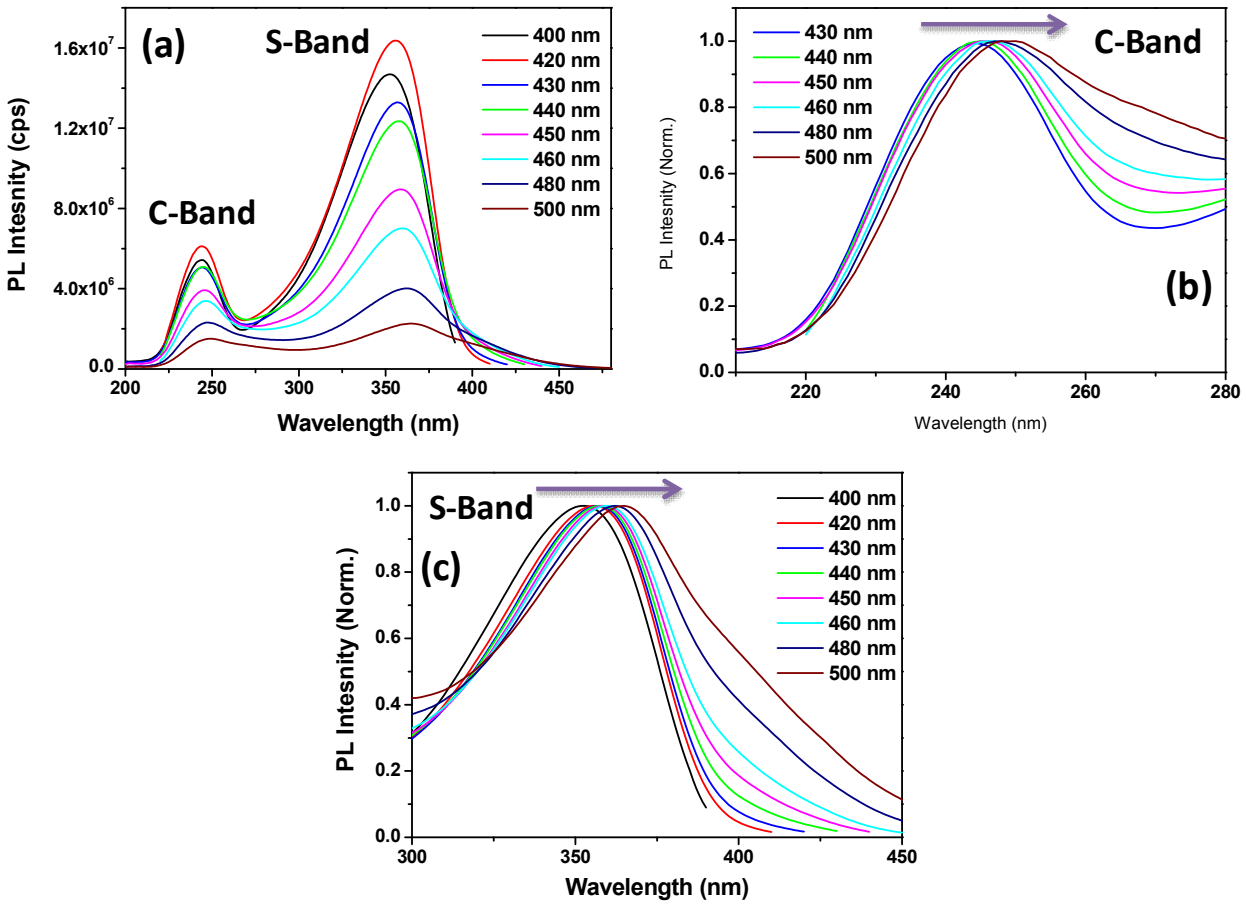

Figure S4. (a) Emission wavelength dependent excitation spectra of N-CDs, (b) Emission wavelength dependent excitation spectra of N-CDs normalized at C-band, (c) Emission wavelength dependent excitation spectra of N-CDs normalized at S-band.

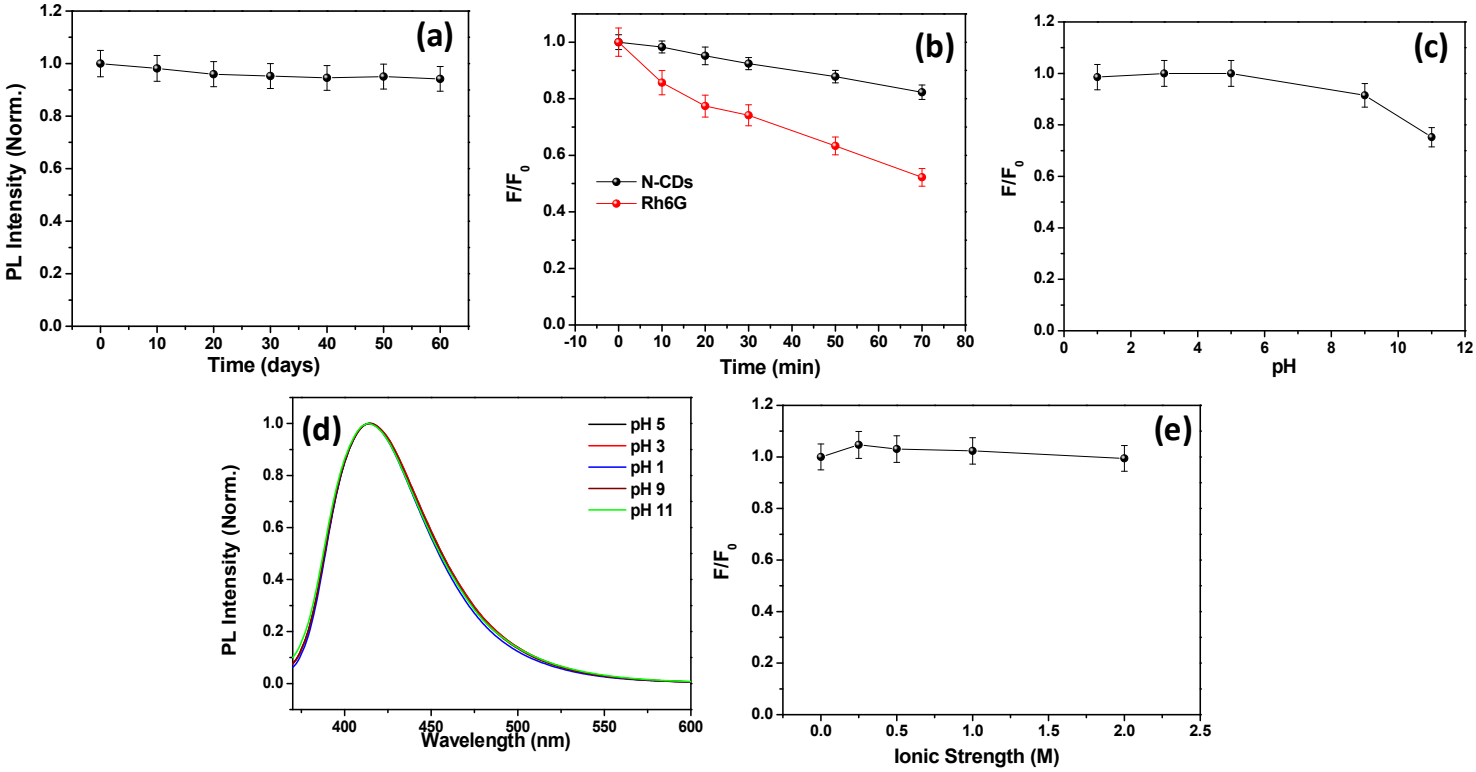

Figure S5. (a) Long-term luminescence stability of N-CDs. Effect of (b) UV irradiation, (c & d) pH, and (e) ionic strength on the luminescence intensity of N-CDs.

Table S5. Comparison of IA-derived N-CDs with previously reported CDs towards the detection of Fe^{3+} ions.

S. No.	Fluorescence Probe	Sensing Mechanism	LOD	Linear range	Ref.
1	CDs	NA	NA	1-100 μM	35
2	N,S-CDs	Complexation followed by photoelectron transfer	NA	NA	20
3	CDs	Complexation followed by non-radiative electron or energy transfer	20 μM	20–200 μM	23
4	N-CDs	Complexation followed by non-radiative electron transfer	17.9 μM	NA	36
5	N-CDs	Electron or energy transfer	10 μM	NA	27
6	N-CDs	Photoelectron transfer	10.8 μM	50–100 μM	37
7	CDs	Dynamic electron transfer	9.97 μM	12.5–100 μM	38
8	CDs	NA	6 μM	0–166 μM	39
9	CDs	Complexation followed by photoelectron transfer	4.67 μM	0–50 μM	26
10	N,S-CDs	Complexation followed by photoelectron transfer	4 μM	25–500 μM	3
11	N-CDs	Combined static and dynamic quenching	2.5 μM	1–90 μM	8
12	CDs	Complexation followed by photoelectron transfer	2 μM	Up to 200 μM	40
13	CDs	Complexation followed by photoelectron transfer	1.3 μM	0–50 μM	4
14	N-CDs	Complexation followed by non-radiative electron or energy transfer	0.96 μM	0–100 μM	7
15	CDs	NA	0.5 μM	NA	35
16	N-CDs	Complexation	0.45 μM	1.6–333.3 μM	25
17	CDs	Complexation	0.4 μM	0–6 μM	15
18	N,P-CDs	Complexation	0.33 μM	1–150 μM	27
19	CDs	Photoelectron transfer	0.31 μM	0–20 μM	41
20	N-CDs	Complexation followed by photoelectron transfer	0.18 μM	0.01–1.8 ppm	28
21	CDs	Complexation followed by photoelectron transfer	0.17 μM	1–100 μM	42

22	CDs	Complexation followed by photoelectron transfer	0.16 μM	0–100 μM	43
23	N-CDs	Complexation followed by non-radiative electron or energy transfer	0.14 μM	0–100 μM	44
24	**N-CDs**	**Complexation followed by photoelectron transfer**	**96 nM**	**0–300 μM**	**This Work**
25	CDs	Aggregation	60 nM	0.2–100 μM	45
26	N,S,P-CDs	Complexation followed by photoelectron transfer	49.6 nM	0.1–6 μM	46
27	CDs	Complexation and ground state electron transfer	35 nM	0–50 μM	47
28	N,S,P-CDs	Complexation followed by photoelectron transfer	31.5 nM	0.1–10 μM	46
29	CDs	Complexation	24.4 nM	0–5.3 μM	48
30	CDs	Complexation followed by dynamic quenching	10 nM	1 nM–100 μM	49

Table S6. Comparison of IA-derived N-CDs with other fluorescence probes reported for the determination of Fe^{3+} ions.

S. No.	Fluorescence Probe	LOD	Linear range	Ref.
1	NPNDs	100 μM	0-30 μM	50
2	GO Nanosheets	17.5 μM	14.3–143.2 μM	51
3	Anthracene-appended amino acids	10 μM	0–1.2 mM	52
3	Anthracene-appended amino acids	10.9 μM	0–1 mM	52
4	GQDs	7.22 μM	0-80 μM	53
5	Au Nanoclusters	3.5 μM	5–1.28 mM	54
6	Rhodamine-based fluorescent chemosensor	1.5 μM	0–20 μM	55
7	Pyrazoline derivative	1.4 μM		56
8	2,5-Diphenylfuran and 8-hydroxyquinoline	0.97 μM	0–150 μM	57
9	MOF Particles	0.90 μM	3–200 μM	58
10	Naphthalimide and coumarin	0.39 μM	12–149 μM	59
11	F-CNPs	0.32 μM	0–20 μM	60
12	Diaza-18-crown-6 ether with dual coumarins	0.31 μM	0–30 μM	61
13	Aminoantipyrine	0.21 μM	1–20 μM	62
14	Ag Nanoclusters	0.12 μM	0.5–20 μM	63
15	**N-CDs**	**96 nM**	**0–300 μM**	**This Work**
16	N-GQDs	80 nM	1–70 μM	18
17	CDs	10 nM	1 nM–100 μM	49

Determination of Limit of Detection (LOD)

The detection limit or limit of detection (LOD) of CDs towards Fe^{3+} was determined as follows:

$$LOD = \frac{K \times Sbl}{S}$$

Where, K = 3, Sb1 is the standard deviation of the blank solution and S is the slope of the calibration curve.The standard deviation (Sbl) for ten subsequent measurements of fluorescence intensities of blank were calculated using the following equation:

$$\sigma = \sqrt{\frac{\Sigma(x - \mu)^2}{N}}$$

Where, σ is standard deviation, *x* is blank measurements, μ is the mean of all ten blank measurements, N is the total number of measurements *viz.* 10.

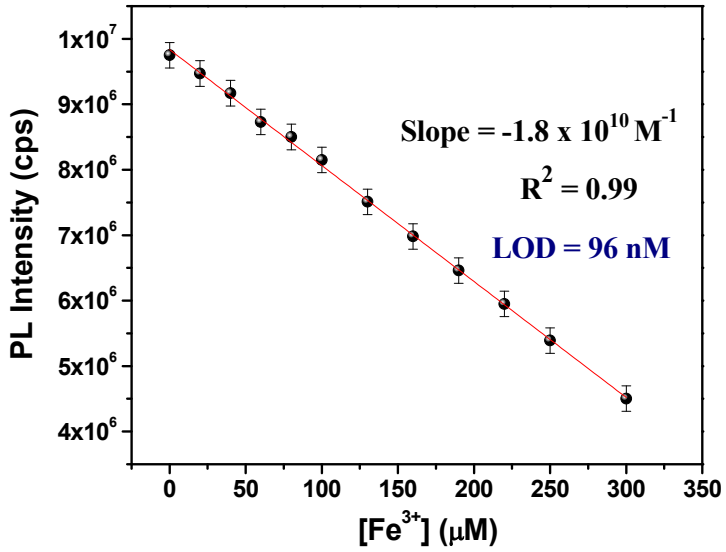

Figure S6. Calibration curve for the fluorimetric detection of Fe^{3+} ions.

Determination of trace Fe^{3+} in various field water samples

Fe^{3+} is selectively complexes with thiocyanate ions to produce a red color iron thiocyanate complex.[64,65] We have utilized this method to determine the concentration of trace Fe^{3+} ions in various field water samples. A series of standard ferric ion solutions were treated with 10 % KSCN solution in presence of 4 M HCl. The solutions are allowed to stand for 5 min to develop a red color. Same procedure is done for field water samples. The absorbance values of all the solutions are measured at 490 nm which is the absorbance of iron thiocyanate complex. A calibration curve is obtained by plotting the known concentrations of standard iron solutions against their absorbance. Then the absorbance values of field water samples are interpolated to obtain their concentrations.

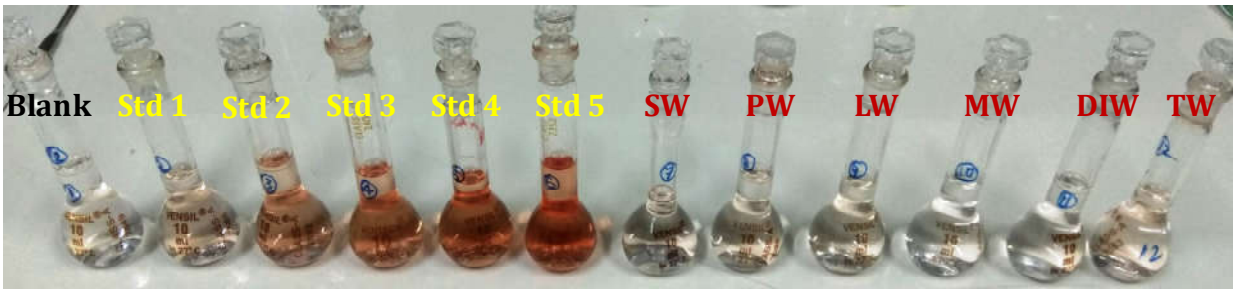

Figure S7. Photographs of standard Fe^{3+} solutions and various field waters on the addition of KSCN

Table S7. Data to obtain the calibration curve for the determination of unknown Fe^{3+} concentration.

Solution	Conc. of Fe^{3+} (ppm)	Absorbance @ 490 nm
Blank	0	0
Standard 1	1	0.029
Standard 2	3	0.120
Standard 3	5	0.212
Standard 4	7	0.315
Standard 5	10	0.478

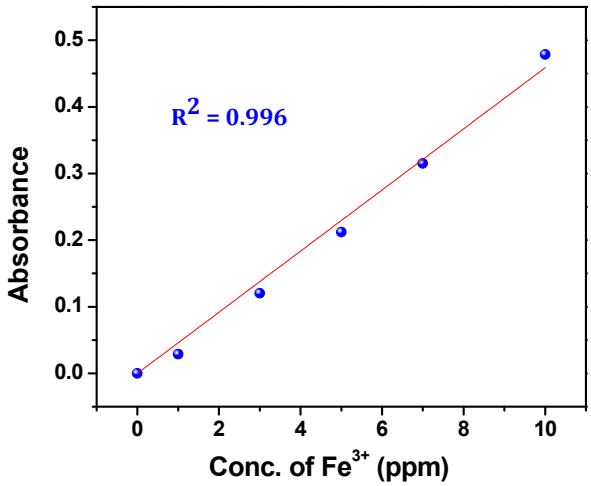

Figure S8. Calibration curve for the determination of unknown Fe^{3+} concentration.

Table S8. Unknown Fe^{3+} concentrations obtained by the interpolation of absorbance values in the calibration curve

Solution	Absorbance @ 490 nm	Interpolated Conc. of Fe^{3+} (ppm)
SW	0.015	0.32
PW	0.038	0.83
LW	0.015	0.32
TW	0.054	1.17
MW	0	0
DIW	0	0

Table S9. Parameters obtained from the fitting of fluorescence decays in the absence and presence of Fe^{3+} ions.

Analyte	τ_1 (ns)	τ_2 (ns)	τ_3 (ns)	A_1 (%)	A_2 (%)	A_3 (%)	τ_{mean} **(ns)**	Red. χ^2
N-CDs	0.53 ± 0.03	2.61 ± 0.05	9.83 ± 0.10	7.35	39.52	53.13	**6.33**	1.13
N-CDs + Fe^{3+}	0.29 ± 0.02	1.34 ± 0.03	4.12 ± 0.04	10.99	45.88	43.13	**2.44**	1.11

References

1. Haijuan Zhang, Yonglei Chen, Meijuan Liang, Laifang Xu, Shengda Qi, Hongli Chen, and Xingguo Chen, Solid-Phase Synthesis of Highly Fluorescent Nitrogen-Doped Carbon Dots for Sensitive and Selective Probing Ferric Ions in Living Cells, *Anal. Chem.,* 2014, **86**, 9846-9852.
2. Jun Di, Jiexiang Xia, Mengxia Ji, Bin Wang, Xiaowei Li, Qi Zhang, Zhigang Chen, and Huaming Li, Nitrogen-Doped Carbon Quantum Dots/BiOBr Ultrathin Nanosheets: In Situ Strong Coupling and Improved Molecular Oxygen Activation Ability under Visible Light Irradiation, *ACS Sustainable Chem. Eng.*, 2016, **4**, 136-146.
3. Hui Ding, Ji-Shi Wei and Huan-Ming Xiong, Nitrogen and sulfur co-doped carbon dots with strong blue luminescence, *Nanoscale*, 2014, **6**, 13817-13823.
4. Ming Zhou, Zhulong Zhou, Aihua Gong, Yan Zhang, Qijun Li, Synthesis of highly photoluminescent carbon dots via citric acid and Tris for iron(III) ions sensors and bioimaging, *Talanta*, 2015, **143**, 107–113.
5. Haimin Zhang, Yibing Li, Xiaolu Liu, Porun Liu, Yun Wang, Taicheng An, Huagui Yang, Dengwei Jing, and Huijun Zhao, Determination of Iodide via Direct Fluorescence Quenching at Nitrogen-Doped Carbon Quantum Dot Fluorophores, *Environ. Sci. Technol. Lett.*, 2014, **1**, 87-91.

6. He Huang, Chunguang Li, Shoujun Zhu, Hailong Wang, Cailing Chen, Zhaorui Wang, Tianyu Bai, Zhan Shi, and Shouhua Feng, Histidine-Derived Nontoxic Nitrogen Doped Carbon Dots for Sensing and Bioimaging Applications, *Langmuir*, 2014, **30**, 13542-13548.
7. Thomas Nesakumar Jebakumar Immanuel Edison, Raji Atchudan, Jae-Jin Shim, Senthilkumar Kalimuthu, Byeong-Cheol Ahn, Yong Rok Lee, Turn-off fluorescence sensor for the detection of ferric ion in water using green synthesized N-doped carbon dots and its bio-imaging, *Journal of Photochemistry & Photobiology, B: Biology*, 2016, **158**, 235–242.
8. Tapas Kumar Mondal, Abhisek Gupta, Bikash Kumar Shaw, Supriya Mondal, Uttam Kumar Ghorai and Shyamal K. Saha, Highly luminescent N-doped carbon quantum dots from lemon juice with porphyrin-like structures surrounded by graphitic network for sensing applications, *RSC Adv*., 2016, **6**, 59927–59934.
9. Mingcong Rong, Yufeng Feng, Yiru Wang, Xi Chen, One-pot solid phase pyrolysis synthesis of nitrogen-doped carbon dots for Fe^{3+} sensing and bioimaging, *Sensors and Actuators B*, 2017, **245**, 868–874.
10. Yongming Guo, Fengpu Cao, Yabo Li, Solid phase synthesis of nitrogen and phosphor co-doped carbon quantum dots for sensing Fe^{3+} and the enhanced photocatalytic degradation of dyes, *Sensors and Actuators B*, 2018, **255**, 1105–1111.
11. Qi Wang, Xing Liu, Lichun Zhang and Yi Lv, Microwave-assisted synthesis of carbon nanodots through an eggshell membrane and their fluorescent application, *Analyst*, 2012, **137**, 5392–5397.
12. Lina Xu, Hao Fan, Lixin Huang, Jianling Xia, Jinrui Huang, Mei Li, Haiyang Ding, Kun Huang, Shouhai Li, Eosinophilic nitrogen-doped carbon dots derived from tribute chrysanthemum for label-free detection of Fe^{3+} ions and hydrazine, *J. Taiwan. Inst. Chem. E*., 2017, **78**, 247–253.
13. Pengfei Lv, Yixin Yao, Dawei Li, Huimin Zhou, Muhammad Awais Naeem, Quan Feng, Jieyu Huang, Yibing Cai, Qufu Wei, Self-assembly of nitrogen-doped carbon dots anchored on bacterial cellulose and their application in iron ion detection, *Carbohydrate Polymers*, 2017, **172**, 93–101.

14. Xiaobiao Cui, Yinglin Wang, Jie Liu, Qiuyue Yang, Bo Zhang, Yuan Gao, Yue Wang, Geyu Lu, Dual functional N- and S-co-doped carbon dots as the sensor for temperature and Fe^{3+} ions, *Sensors and Actuators B*, 2017, **242**, 1272–1280.
15. Abhay Sachdev and P. Gopinath, Green synthesis of multifunctional carbon dots from coriander leaves and their potential application as antioxidants, sensors and bioimaging agents, *Analyst,* 2015, **140**, 4260–4269.
16. Yanfen Chen, Yuanya Wu, Bo Weng, Bin Wang, Changming Li, Facile synthesis of nitrogen and sulfur co-doped carbon dots and application for Fe(III) ions detection and cell imaging, *Sensors and Actuators B*, 2016, **223**, 689–696.
17. Yongqiang Dong, Hongchang Pang, Hong Bin Yang, Chunxian Guo, Jingwei Shao, Yuwu Chi, Chang Ming Li, and Ting Yu, Carbon-Based Dots Co-doped with Nitrogen and Sulfur for High Quantum Yield and Excitation-Independent Emission, *Angew. Chem. Int. Ed*., 2013, **52**, 7800 –7804.
18. Hongbo Xu, Shenghai Zhou, Lili Xiao, Huanhuan Wang, Shouzhu Li and Qunhui Yuan, Fabrication of a nitrogen-doped graphene quantum dot from MOF-derived porous carbon and its application for highly selective fluorescence detection of Fe^{3+}, *J. Mater. Chem. C*, 2015, **3**, 291–297.
19. Zhi Yang, Minghan Xu, Yun Liu, Fengjiao He, Feng Gao, Yanjie Su, Hao Wei and Yafei Zhang, Nitrogen-doped, carbon-rich, highly photoluminescent carbon dots from ammonium citrate, *Nanoscale*, 2014, **6**, 1890–1895.
20. Yupeng Sun, Chen Shen, Jing Wang and Yun Lu, Facile Synthesis of Biocompatible N, S-doped Carbon Dots for Cell Imaging and Ion Detecting, *RSC Adv.*, 2015, **5**, 16368-16375.
21. Zicheng Liang, Lei Zeng, Xiaodong Cao, Qun Wang, Xiaohui Wang, and Runcang Sun, Sustainable Carbon Quantum Dots from Forestry and Agricultural Biomasswith AmplifiedPhotoluminescence by Simple NH_4OH Passivation, *J. Mater. Chem. C*, 2014, **2**, 9760-9766.
22. Bingfang Shi, Yubin Su, Liangliang Zhang, Mengjiao Huang, Rongjun Liu, and Shulin Zhao, Nitrogen and Phosphorus Co-Doped Carbon Nanodots as a Novel Fluorescent Probe for Highly Sensitive Detection of Fe^{3+} in Human Serum and Living Cells, *ACS Appl. Mater. Interfaces*, 2016, **8**, 10717-10725.

23. Soumen Chandra, Dipranjan Laha, Arindam Pramanik, Angshuman Ray Chowdhuri, Parimal Karmakar and Sumanta Kumar Sahu, Synthesis of highly fluorescent nitrogen and phosphorus doped carbon dots for the detection of Fe^{3+} ions in cancer cells, *Luminescence*, 2016, **31**, 81–87.
24. Chengkun Jiang, Hao Wu, Xiaojie Song, Xiaojun Ma, Jihui Wang, Mingqian Tan, Presence of photoluminescent carbon dots in Nescafe original instant coffee: Applications to bioimaging, *Talanta*, 2014, **127**, 68–74.
25. Long Wang, Juan Hou, Huiyu Li, Qi Zhao, Fengshuang Zhang, Jiahui Zhao, Hong Ding, Lan Ding, Facile synthesis of nitrogen-doped carbon dots and its application as sensing probes for serum iron, *J Nanopart Res*, 2015, **17**, 457–468.
26. Jing Yu, Chunxiang Xu, Zhengshan Tian, Yi Lin and Zengliang Shi, Facilely synthesized N-doped carbon quantum dots with high fluorescent yield for sensing Fe^{3+}, *New J. Chem.,* 2016, **40**, 2083–2088.
27. Guili He, Minghan Xu, Mengjun Shu, Xiaolin Li, Zhi Yang, Liling Zhang, Yanjie Su, Nantao Hu and Yafei Zhang, Rapid solid-phase microwave synthesis of highly photoluminescent nitrogen-doped carbon dots for Fe^{3+} detection and cellular bioimaging, Nanotechnology, 2016, 27, 395706–395716.
28. Jingfang Shangguan, Jin Huang, Dinggeng He, Xiaoxiao He, Kemin Wang, Runzhi Ye, Xue Yang, Taiping Qing, and Jinlu Tang, Highly Fe^{3+}-Selective Fluorescent Nanoprobe Based on Ultrabright N/P Codoped Carbon Dots and Its Application in Biological Samples, *Anal. Chem*., 2017, **89**, 7477-7484.
29. Xiaojuan Gong, Wenjing Lu, Man Chin Paau, Qin Hu, Xin Wu, Shaomin Shuang, Chuan Dong, Martin M.F. Choi, Facile synthesis of nitrogen-doped carbon dots for Fe^{3+} sensing and cellular imaging, *Analytica Chimica Acta*, 2015, **861,** 74–84.
30. Jing Liu, Xinling Liu, Hongjie Luo and Yanfeng Gao, One-step preparation of nitrogen-doped and surface-passivated carbon quantum dots with high quantum yield and excellent optical properties, *RSC Adv*., 2014, **4**, 7648–7654.
31. Cuiping Han, Ru Wang, Keying Wang, Huiting Xu, Meirong Sui, Jingjing Li, Kai Xu, Highly fluorescent carbon dots as selective and sensitive “on-off-on” probes for iron(III) ion and apoferritin detection and imaging in living cells, *Biosensors and Bioelectronics*, 2016, **83**, 229–236.

32. Wentai Wang, Tak Kim, Zifeng Yan, Guangshan Zhu, Ivan Cole, Nam-Trung Nguyen, Qin Li, Carbon dots functionalized by organosilane with double-sided anchoring for nanomolar Hg^{2+} detection, *Journal of Colloid and Interface Science*, 2015, **437**, 28–34.
33. Qingxiu Yang, Lin Wei, Xuanfang Zheng & Lehui Xiao, Single Particle Dynamic Imaging and Fe^{3+} Sensing with Bright Carbon Dots Derived from Bovine Serum Albumin Proteins, *Sci. Rep.*, 2015, **5**, 17727–17739.
34. Reference 8 in the main article.
35. Liangliang Zhu, Yongjin Yin, Cai-Feng Wang and Su Chen, Plant leaf-derived fluorescent carbon dots for sensing, patterning and coding, *J. Mater. Chem. C*, 2013, **1**, 4925–4932.
36. Shoujun Zhu, Qingnan Meng, Lei Wang, Junhu Zhang, Yubin Song, Han Jin, Kai Zhang, Hongchen Sun, Haiyu Wang, and Bai Yang, Highly Photoluminescent Carbon Dots for Multicolor Patterning, Sensors, and Bioimaging, *Angew. Chem. Int. Ed.*, 2013, **52**, 3953–3957.
37. Guangming Li, Nan Lv, Wenzhi Bi, Jilin Zhang and Jiazuan Ni, Nitrogen-doped carbon dots as a fluorescence probe suitable for sensing Fe^{3+} under acidic conditions, *New J. Chem.***,** 2016, **40**, 10213–10218.
38. Ayşe Merve Aslandaş, Neslihan Balcı, Mustafa Arık, Halis Şakiroğlu, Yavuz Onganer, and Kadem Meral, Liquid nitrogen-assisted synthesis of fluorescent carbon dots from *Blueberry* and their performance in Fe^{3+} detection, *Applied Surface Science*, 2015, **356**, 747–752.
39. Hamed Hamishehkar, Bahar Ghasemzadeh, Abdolhossein Naseri, Roya Salehi, Farzaneh Rasoulzadeh, Carbon dots preparation as a fluorescent sensing platform for highly efficient detection of Fe(III) ions in biological systems, *Spectrochimica Acta Part A: Molecular and Biomolecular Spectroscopy*, 2015, **150**, 934–939.
40. Yubin Song, Shoujun Zhu, Siyuan Xiang, Xiaohuan Zhao, Junhu Zhang, Hao Zhang, Yu Fu and Bai Yang, Investigation into the fluorescence quenching behaviors and applications of carbon dots, *Nanoscale*, 2014, **6**, 4676-4682.
41. Rajkumar Bandi, Bhagavanth Reddy Gangapuram, Ramakrishna Dadigala, Ravikumar Eslavath, Surya S. Singh and Veerabhadram Guttena, Facile and green synthesis of

fluorescent carbon dots from Onion waste and their potential applications as sensor and multicolour imaging agents, *RSC Adv.*, 2016, **6**, 28633-28639.

42. M. Reza Hormozi-Nezhad and M. Taghipour, Quick speciation of iron(II) and iron(III) in natural samples using a selective fluorescent carbon dot-based probe, *Anal. Methods*, 2016, **8**, 4064-4068.
43. Namasivayam Dhenadhayalan & King-Chuen Lin, Chemically Induced Fluorescence Switching of Carbon-Dots and Its Multiple Logic Gate Implementation, *Sci. Rep*., 2015, **5**, 10012.
44. Shaoqing Liu, Ruili Liu, Xia Xing, Chongqing Yang, Yi Xu and Dongqing Wu, Highly Photoluminescent Nitrogen-Rich Carbon Dots from Melamine and Citric Acid for Selective Detection of Iron(III) Ion, *RSC Adv.*, 2016, **6**, 31884-31888.
45. Tzu-Heng Chen and Wei-Lung Tseng, Self-Assembly of Monodisperse Carbon Dots into High-Brightness Nanoaggregates for Cellular Uptake Imaging and Iron(III) Sensing, *Anal. Chem.*, **2017**, *89* (21), pp 11348–11356.
46. Lizhen Liu, Feng Feng, Man Chin Paau, Qin Hu, Yang Liu, Zezhong Chen and Martin M. F. Choi, Carbon dots isolated from chromatographic fractions for sensing applications, *RSC Adv*., 2015, **5**, 106838-106847.
47. Anam Iqbal, Yuejun Tian, Xudong Wang, Deyan Gong, Yali Guo, Kanwal Iqbal, Zhiping Wang, Weisheng Liu, Wenwu Qin, Carbon dots prepared by solid state method via citric acid and 1,10-phenanthroline for selective and sensing detection of Fe^{2+} and Fe^{3+}, *Sensors and Actuators B*, 2016, **237**, 408–415.
48. Xuting An, Shujuan Zhuo, Ping Zhang and Changqing Zhu, Carbon dots based turn-on fluorescent probes for oxytetracycline hydrochloride sensing, *RSC Adv.*, 2015, **5**, 19853-19858.
49. Chuanxi Wang, Yijun Huang, Kaili Jiang, Mark G. Humphrey and Chi Zhang, Dual-emitting quantum dot/carbon nanodot-based nanoprobe for selective and sensitive detection of Fe^{3+} in cells, *Analyst,* 2016, **141**, 4488–4494.
50. Tiantian Lai, Enhui Zheng, Lixian Chen, Xuyang Wang, Lichun Kong, Chunping You, Yongming Ruan and Xuexiang Weng, Hybrid carbon source for producing nitrogen-doped polymer nanodots: one-pot hydrothermal synthesis, fluorescence enhancement and highly selective detection of Fe(III), *Nanoscale*, 2013, **5**, 8015–8021.
51. Dong Wang, Lei Wang, Xinyi Dong, Zhun Shi, Jian Jin, Chemically tailoring graphene oxides into fluorescent nanosheets for Fe^{3+} ion detection, *Carbon*, 2012, **50**, 2147–2154.

52. Lohani, C. R.; Kim, J. M.; Lee, K. H. Facile Synthesis of Anthracene-appended Amino Acids as Highly Selective and Sensitive Fluorescent Fe^{3+} Ion Sensors. *Bioorg. Med. Chem. Lett*., 2009, **19**, 6069-6073.
53. Arundithi Ananthanarayanan, Xuewan Wang, Parimal Routh, Barindra Sana, Sierin Lim, Dong-Hwan Kim, Kok-Hwa Lim, Jun Li, Peng Chen, Facile Synthesis of Graphene Quantum Dots from 3D Graphene and their Application for Fe^{3+} Sensing, *Adv. Funct. Mater*., 2014, **24**, 3021–3026.
54. Ja-an Annie Ho, Heng-Chia Chang, and Wen-Ta Su, DOPA-Mediated Reduction Allows the Facile Synthesis of Fluorescent Gold Nanoclusters for Use as Sensing Probes for Ferric Ions, *Anal. Chem*., 2012, **84**, 3246–3253.
55. Wang J, Zhang D, Liu Y, Ding P, Wang C, Ye Y, Zhao Y A, N-stablization rhodamine-based fluorescent chemosensor for Fe^{3+} in aqueous solution and its application in bioimaging. *Sens Actuators B*, 2014, **191**, 344–350.
56. Shengli Hu, Shushu Zhang, Chan Gao, Caihua Xu, Qing Gao. A New Selective Fluorescent Sensor for Fe^{3+} Based on a Pyrazoline Derivative, *Spectrochim. Acta, Part A* 2013, **113**, 325-331.
57. Shengli Hu, Gongying Wu, Caihua Xu, Jinghua Dong, Qing Gao, A New Fluorescent Chemosensor for Fe^{3+} Based upon 2,5-Diphenylfuran and 8- Hydroxyquinoline. *J. Photochem. Photobiol., A*, 2013, **270**, 37-42.
58. Cheng-Xiong Yang, Hu-Bo Ren, and Xiu-Ping Yan, Fluorescent Metal–Organic Framework MIL-53(Al) for Highly Selective and Sensitive Detection of Fe^{3+} in Aqueous Solution, *Anal. Chem*., 2013, **85**, 7441–7446.
59. Zhengqian Li, Ying Zhou, Kai Yin, Zhu Yu, Yan Li, and Jun Ren, A new fluorescence ‘‘turn-on’’ type chemosensor for Fe^{3+} based on naphthalimide and coumarin. *Dyes Pigments,* 2014, **105**, 7–11.
60. Songnan Qu, Hong Chen, Xuanming Zheng, Junsheng Cao, and Xingyuan Liu, Ratiometric fluorescent nanosensor based on water soluble carbon nanodots with multiple sensing capacities, *Nanoscale*, 2013, **5**, 5514–5518.
61. Li H, Li L, Yin B Highly selective fluorescent chemosensor for Fe^{3+} detection based on diaza-18-crown-6 ether appended with dual coumarins. *Inorg Chem Commun,,* 2014, **42**, 1–4.

62. Yanmei Zhou, Hua Zhou, Junli Zhang, Lin Zhang, Jingyang Niu, Fe^{3+}-Selective Fluorescent Probe Based on Aminoantipyrine in Aqueous Solution. *Spectrochim. Acta, Part A*, 2012, **98**, 14-17.
63. Zhen Chen, Dongtao Lu, Guomei Zhang, Jun Yang, Chuan Dong, and Shaomin Shuang, Glutathione capped silver nanoclusters-based fluorescent probe for highly sensitive detection of Fe^{3+}, *Sens. Actuators B*, 2014, **202**, 631–637.
64. Determination of thiocyanate using iron(III), RSC Student Worksheet, www.rsc.org/learn-chemistry/resource/download/res00000906/cmp00001181/pdf.
65. What's in the water: Determination of iron. Ryerson University Lab booklet. https://www.ryerson.ca/content/dam/osoe/High-School-Images/Activity-Info/OSOEChemInfo.pdf.